Techset Composition Ltd, Salisbury
Doc: {IEE}RSN/Articles/Pagination/RSNSI20140206.3d

www.ietdl.org

Published in IET Radar, Sonar and Navigation
Received on 30th April 2014
Revised on 7th August 2014
Accepted on 14th October 2014
doi: 10.1049/iet-rsn.2014.0206

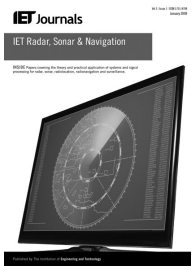

ISSN 1751-8784

Experimental investigation into radar-based central blood pressure estimation

Lars Erik Solberg[1], Øyvind Aardal[2], Tor Berger[2], Ilangko Balasingham[1,3], Erik Fosse[1,4], Svein-Erik Hamran[2,5]

[1]*Interventional Centre, Oslo University Hospital, Oslo 0424, Norway*
[2]*Norwegian Defence Research Establishment, PO Box 25, Kjeller 2027, Norway*
[3]*Department of Electronics and Telecommunications, Norwegian University of Science and Technology (NTNU), Trondheim 7491, Norway*
[4]*Institute of Clinical Medicine, University of Oslo, Oslo 0424, Norway*
[5]*Department of Informatics, University of Oslo, PO Box 1080 Blindern, Oslo 0316, Norway*
E-mail: lars.erik.solberg@gmail.com

Abstract: To assess whether radar technology can be used for monitoring blood pressure via information from the aorta, two experiments were performed: (i) measurements on a phantom model and (ii) acquisitions on a human subject for in vivo experiments. A linear dependency of phase on radius in the radar echoes in the phantom model showed that the information regarding the radius of a circular, cylindrical object depended on the clutter environment: in a low-clutter case two distinct reflections were identified, whereas in the high-clutter case it was possible to extract a proxy. Radar echoes from antennas strapped to the back of a human subject showed a clear signature from a discernible, distinct reflector believed to be the aorta. However, as for the high-clutter case, only a proxy for aortic radius is available as basis for estimation, which is most likely coupled with aortic displacements.

1 Introduction

Vital signs, like blood pressure and pulse, are the most commonly used tests in all patients. Blood pressure can be obtained by an external cuff or by intra-arterial measurement through a cannula. The present study was performed in order to see if a radar placed outside the patient can be used to measure blood pressure and pulse.

Current devices for non-invasive measurements of blood pressure include the sphygmomanometer, photoplethysmograph [1], tonography [2] and pulse transit time [3]. However, they all rely on peripheral measurement points. This may constitute a problem in certain situations such as when flow redistribution to central parts of the body (heavy injury, temperature etc.) degrades these measurements; another situation where central measurements may prove advantageous is during the presence of strong movements of the peripheral locations which affect pressure measurements [4].

The use of radar-based approaches in a medical context is neither new nor common [5]. In the past decade, research into the use of radar techniques for medical purposes has concentrated on two main objectives: estimating the pulse and respiration rate in varying situations and at a distance from the subject, typically in the context of continuous, non-contact monitoring, and microwave imaging of the breast for the early detection of breast tumours.

Our aim was to investigate whether a radar could be used to estimate the blood pressure in the aorta. There seems to be two possible approaches (Fig. 1)

Method 1: Sugawara *et al.* [6] showed a linear relationship between percentage changes in instantaneous blood pressure and diameter of the carotid artery.

Method 2: According to [3, 4, 7] there is a non-linear relationship between mean arterial blood pressure ($\bar{P}$) and compliance (ratio of change in volume for a change in pressure), which in turn is related to pulse wave velocity (PWV).

Common to these approaches, the radar-based method will need measures of the aortic radius as a function of time ($r(t)$). In Method 1, the radius of the aorta would be estimated based on any location along its trunk, and this radius would be related to the pressure. In Method 2, any common marker related to $r(t)$ at two distinct points along the aorta with known separation L could be used to estimate the delay T and thereby the PWV. PWV would in turn lead to a blood pressure estimate. The required precision is different: in the latter approach, the actual radius is not used directly, but rather its profile through the heart cycle at different locations, see Fig. 1.

The Method 2 essentially requires each pulse to be detected, along with their exact timing. Then two points would be compared. The detection of arterial pulses has been addressed in the literature: arterial distensions using waveguides in [8, 9]; contactless heart movement measurements in [10]; source analysis of heart echoes in [11]; and pulse transit time estimation in [12, 13]. These approaches use heart movements

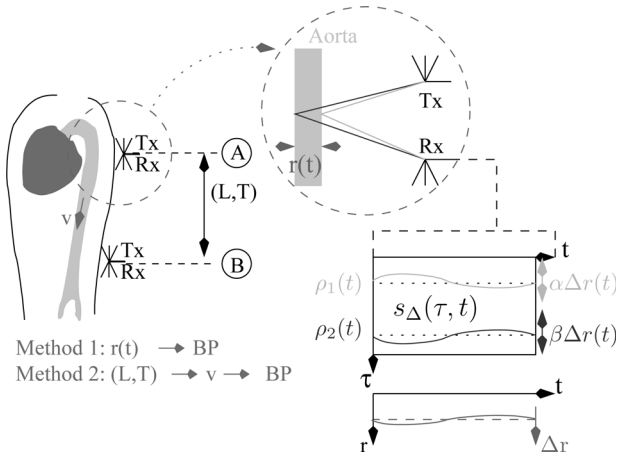

Fig. 1 *Blood pressure estimation methods*

At A and B, a series of dynamic echoes $s_\Delta(\tau, t)$ are captured and contain information regarding moving reflectors. $\rho_1(t)$ and $\rho_2(t)$ represent two such reflectors, which are related to the aorta radius $r(t)$ with sensitivities α, β. T is the delay of the pulse between the points A and B, with internal distance L

or observe peripheral arteries such as the radial, carotid or femoral arteries. Basing estimation on the aorta in this study distinguishes it from the aforementioned studies. This approach is potentially more specific: properties of the arterial tree would be averaged when combining peripheral points with the heart. Furthermore, as mentioned above, there are situations where the peripheral location's pressure may be affected.

The diameter variations in the aorta were measured by Stefanidis [14] using a precise and invasive method based on pressure and diameter sensors introduced through catheters. He concluded that typical radius peak-to-peak amplitudes for a normal population was 1.09 ± 0.22 mm.

The primary objective of the present study was to determine whether the information relating to the aortic radius could be extracted from radar measurements. Second, we aimed at determining whether this information could be used to estimate changes in blood pressure. As such we have not addressed practical issues such as body movement or respiration. Certain applications (e.g. device in a stretcher or chair) may reduce the first through a tight coupling between antenna and body. Although important and challenging, these issues lie outside the scope of this paper.

The study was conducted in three stages: first, we studied radius estimation in a phantom model with and without clutter sources; second, potential error sources in human subject experiments were studied and excluded; and third, experiments with a human subject were performed.

A key issue addressed in this paper was potential clutter sources. Although the radar echoes constituted one source of evidence, we have referred to a concurrent study [15] using magnetic resonance (MR) imaging in order to provide added support for interpreting the radar data.

2 Terminology

The system's coordinate axes were defined as a right-hand system and seen from the back: transverse (x) from left to right, depth (y) from posterior (back) to anterior (front) and longitudinal (z) from lower back towards the neck. Thus, the posterior wall of the aorta was at smallest depth y and the anterior was at largest depth, which corresponded to the first and second reflections from the aorta, respectively.

Radar acquisitions were considered as functions of two variables, where the second variable was an index referring either to radius (r) or time (t). Each indexed value of an acquisition was called an 'echo' ($s(\tau, \cdot)$). The first variable was called 'delay' (τ in s), 'range' (R in m) or frequency (f in Hz) depending on the domain

$$s(\tau, \cdot) = s(2R/c, \cdot) \overset{\text{FT}}{\longleftrightarrow} S(f, \cdot)$$

Here, c refers to a hypothetical, average electromagnetic propagation speed, and because the environment is heterogeneous, the range R does not generally refer to the precise position of a reflector. In general, capitalised variables implicitly indicated the frequency domain. Every echo contained 'reflections' from the environment; some of these were treated as 'reflectors', whereas the remaining variation in observations was referred collectively as 'clutter'.

The 'dynamic echo' (s_Δ) is referred to either a difference with a reference echo, or else a high-pass filtered echo: in both cases, the dynamic echo only depended on that part of the environment which was subject to change. The observation of a delay bin in the dynamic echo as a function of time was called a 'trace' ($p_\tau(t) = s_\Delta(\tau, t)$).

When an imaging algorithm was applied to the dynamic echoes, the term 'dynamic image' ($I_\Delta(x, y, t)$) was used. This algorithm operated on a set of antenna positions: the acquisition at each position was referred to as a 'channel'.

The term 'sensitivity' designated the ratio of a range shift in an echo to a change of geometry, for instance, the range associated with the reflection from the aorta's posterior wall relative to the change in aorta radius.

3 Methods

3.1 Phantom model

The objective of the phantom model was to emulate the use of radar echoes to infer information about the aorta dilatations in an environment similar to the real situation. The phantom model was constructed based on a rubber tube emulating the aorta, filled with water as blood, inserted into a tub filled with a liquid emulating 'average' characteristics of human tissues and of arbitrary objects emulating the heterogeneous environment (Fig. 2). The 'average tissue' was used in [16] to simplify the geometry while retaining the key properties, and an approximation was proposed based on a convex sum of permittivities where weights were based on tissue areas.

For the liquid, we used a mixture of Diacetin and water in the ratio (2:1). With respect to propagation speed, the liquid came close to the average tissue, especially in the region around 1–1.5 GHz where attenuation was weaker, and therefore where similarity was most important; the average ratio c_0/c is 4.86. However, the Diacetin–water mixture had stronger attenuation, and more so with increasing frequency. Beyond 2 GHz, given the round-trip distance to the tube, virtually no relevant information remained in measurements; for this reason, the frequency domain data are tapered and truncated to exclude data above 2 GHz while avoiding ringing associated with simple truncations. The tapering used Hanning window transitions.

The blood pressure estimation should be based on variations in the aortic radius as a function of time. Given the large propagation speed of electromagnetic waves, we assumed that for each radar pulse, tissue displacements

doi: 10.1049/iet-rsn.2014.0206

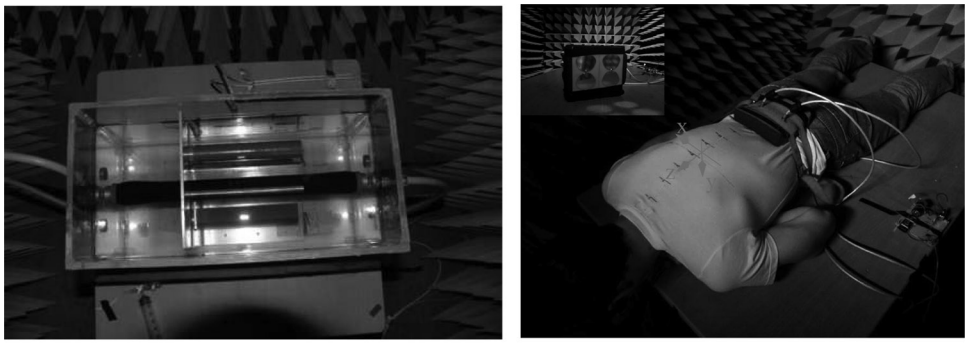

a b

Fig. 2 *Phantom model*

Phantom model (a) with rubber tube at centre and surrounded by clutter objects. Antennas taped to top wall. For the human subject experiments in this paper (b), the antenna couple was strapped to the origin of the coordinate system (drawn in red) **Q5**

would be negligible: a sequence of radar pulses would correspond to sampling the aortic radius. The question hence is whether this radius can be estimated with sufficient precision so that the range of radii will be resolved. For this reason, we considered that it is sufficient to have a static model for each measurement, and vary the radius between them, so as to span a sufficient range. The procedure was:

I) Filling the tub without tube to a set level.
II) Recording the 'background' echo.
III) Insertion of the tube and adjusting the liquid to set level.
IV) Manually measuring the radius of the tube (ca. 1.45 cm for 'simple' and 1.4 cm for 'multiple').
V) Recording the echo.
VI) Injection of ΔV (25 ml) into the rubber tube; the radius after injection was based on calculations ($\Delta r \in \langle 0.40, 0.57 \rangle$ mm).
VII) Removal of ΔV of liquid from the tank (thereby keeping the surface at the same level).
Q4 VIII) Repeated 5 through 7 for the set of radii.

In the two phantom sets, with and without clutter objects, the number of radii differed – but the radius difference between consecutive points remained approximately constant.

A standard experimental approach uses a vector network analyser (VNA) to emulate a radar. Such a device can be used to acquire the transfer function, one frequency at a time, between antennas with high precision and dynamic range. If during the time of an acquisition, the environment can be assumed to be stationary, then through the Fourier transform, the impulse response of the system is calculated, which based on an appropriate signal representation can be considered to be the 'echo' of the radar.

We acquired frequencies between 100 MHz and 5 GHz at steps of 10 MHz and with a 10 Hz internal bandwidth (maximise signal-to-noise ratio and dynamic range): this provided an impulse response with unambiguous range of 100 ns. The recordings were acquired in a small, anechoic chamber. The different experiments used slightly differing antennas with lower 3-dB cut-off frequencies between 0.6 and 1.2 GHz.

In the 'simple geometry', no clutter object was introduced into the tank. In the 'multiple clutter objects' experiment, an arbitrary set of additional objects was introduced: a collection of plastic and metallic cylindrical objects parallel to the 'aorta'. By introducing clutter we investigated the effect of multiple paths although the model did not resemble the human body where diffraction, rather than reflection, may be important.

The VNA dynamic frequency measurements $S_\Delta(f, r)$ were then post-processed to create the dynamic echo s_Δ and the phase difference $\Delta\theta$ relative to a reference radius r_0 of the analytic signal.

$$s_\Delta(\tau, r) = \mathrm{FT}^{-1}\left\{S_\Delta(f, r) \cup \overline{S_\Delta(-f, r)}\right\}$$

$$\theta(\tau, r) = \mathrm{angle}\left(\mathrm{FT}^{-1}\left\{S_\Delta(f, r)\right\}\right)$$

$$\Delta\theta(\tau, r) = \theta(\tau, r) - \theta(\tau, r_0)$$

The phase difference $\Delta\theta$ was, by analogy, interpreted as the delay change of a reflector: a real symmetric bandpass signal ($X(f) \in \mathbb{R}$; $X(f_c + \Delta f) = X(f_c - \Delta f)$), reflected off an ideal point reflector subject to a delay shift $\Delta\tau$, has an analytic representation with $\theta_x(\tau) = \omega_c(\tau - \Delta\tau)$. For this reason, this phase difference was scaled (by $F = -c/(2\omega_c)$) to correspond to an equivalent shift in range.

3.2 Human subject experiments

For these experiments, the subject lay in a prone position on a table with the antenna couple strapped to the back. The VNA swept frequencies from 0.5 to 3 GHz at 50 MHz intervals and with a 10 kHz bandwidth resulting in 51 points and an unambiguous range of 20 ns. A small acquisition time resulted in a maximum sweep rate of approximately 50 Hz, for 20 s with suspended respiration; the heart rate during measurements was close to 1 pulse per second. The measurements were recorded in a small, anechoic chamber and a pad of high-loss material increased isolation of the antennas against the external environment.

3.2.1 Error sources experiments: Given the complex propagation environment, a set of experiments were conducted to address competing hypotheses as explanatory factors of the variations observed in the echoes. These experiments are:

I) 'Transversal': a set of acquisitions along the transverse (x) axis at 0.5 cm intervals covering 3.5 cm to both sides of the origin.
II) 'Longitudinal': a set of acquisitions along the longitudinal (z) axis of the subject at 0.5 cm intervals covering 1.5 cm to both sides of the origin.
III) 'Attaching': a set of acquisitions at the origin while cycling the process of attaching the antenna couple.

IV) 'Equipment': a set of acquisitions at the origin while cycling the process of assembling elements of the equipment (antennas, amplifiers etc.).
V) 'External reflector': a set of acquisitions at the origin with a metallic lid placed in close proximity to the antennas at different positions and representing a 'large' reflector.
VI) 'Respiration': a set of acquisitions at the origin while the degree of inhalation was varied.

To quantify these variations, the average power over time t of the dynamic echoes (s_Δ) was calculated by

$$P_\Delta(\tau) = \frac{1}{T}\sum_{t=t_0}^{t_1} |s_\Delta(\tau, t)|^2 = \mathrm{VAR}_t[s_\Delta(\tau, t)]$$

$$\sigma_s(\tau) = \sqrt{P_\Delta(\tau)} = \mathrm{STD}_t[s_\Delta(\tau, t)]$$

In the following, the use of σ_s was preferred and this was denoted as the 'dynamic density'. Variations in the dynamic density were used to compare the influence of factors on acquisitions: the stronger the factor, the greater the variation in the set of acquisitions defining an experiment.

3.3 Radar imaging

The imaging was based on the method described in [17], and which combined the fast marching algorithm to calculate the shortest round-trip delay $\tau_i(x, y)$ from transmitter to receiver through point (x, y), and the back projection of measurements from the echos $\{s(\tau_i(x, y), t)\}$ to a point (x, y) in the image domain.

$$I_\Delta(x, y, t) = \sum_i s_{\Delta,i}(\tau_i(x, y), t) \quad (1)$$

where $\{i\}$ indexes the set of channels. The fast marching algorithm uses a map of propagation speed $c(x, y)$ (Fig. 3). The map was based on a grossly segmented MR sliced into 'lungs', 'muscle/heart', 'blood', 'bone' and 'fat'. Each region was assigned the corresponding propagation speed, as proposed by Gabriel and Gabriel [18]. Finally, this map was smoothed in order to reduce the dependency of results on the actual choice of MR slice. The contrast at tissue boundaries indicates the strength of reflection of electromagnetic waves at those boundaries.

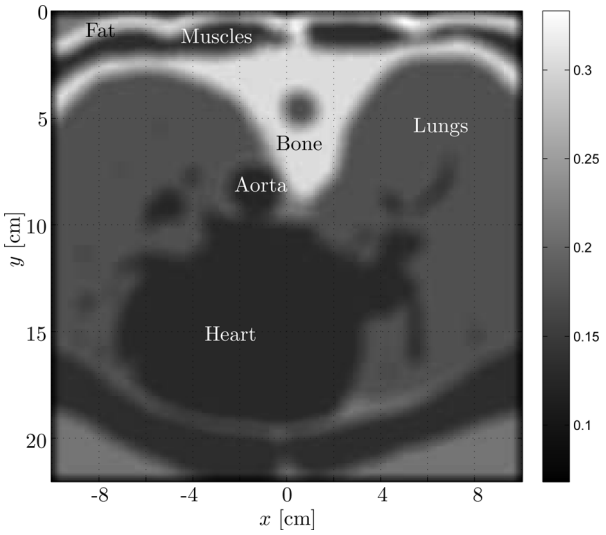

Fig. 3 *Relative velocity map ($c(x, y)/c_0$) used in radar imaging*

An important operation prior to constructing images was synchronising the radar acquisitions, as these were recorded independent of one another. The synchronisation was based on the dynamic echoes where information relative to the heart cycle was evident: the intersection of the steepest slope with the average level of each cycle ('radar cycle marker'). After this operation, the sum in (1) was assumed to accumulate echoes from the same cycle index.

Owing to lack of simultaneous electrocardiogram (ECG) measurements, the results describing the temporal relationship between the radar cycle marker and the ECG QRS complex from prior experiments under identical conditions were assumed valid during these acquisitions. These results showed that the radar cycle marker lags the ECG QRS complex by 0.23 ± 0.1 cycles. The dynamic echoes were quasi-periodic, because they were directly related to the heart beats.

3.4 Extraction of the dynamic signal

For the phantom model experiments, the dynamic echo was constructed as

$$s_\Delta(\tau, r) = s(\tau, r) - s_0(\tau)$$

where $s_0(\tau) = s(\tau, r_0)$ and r_0 was chosen as the smallest of the radii. For the human subject experiments, the dynamic echo was based on a filtering operation

$$s_\Delta(\tau, t) = H_\Delta[s(\tau, t)]$$

The filter H_Δ was a de-trending operation: the subtraction of a low-dimensional polynomial fit from the original data.

3.5 Magnetic resonance (MR) images

To support the analysis of the human subject experiments, MR images were recorded in similar conditions as for the radar acquisitions: prone position of the same individual. However, the respiration was not suspended, rather the MR images in a cine sequence (movie) were acquired at near-maximal exhalation. The analysis of these MR images is described in a separate paper [15], which discusses organ boundary movements in general and the aorta behaviour in particular.

4 Results

4.1 Phantom measurements

In the aim of blood pressure estimation via observations of the aorta dilatations, we chose to study the behaviour in a phantom model, described in the previous section, to address questions relating to the quality of the aorta signature and to the estimation of the aortic radius. Of particular interest was to check whether reliable information of both posterior and anterior aorta reflections were present in observations.

4.1.1 Simple geometry: The dynamic echoes were composed of two reflections distinguished by their positive and negative sensitivities (see Figs. 4 and 5; negative sensitivity shown as neighbouring red, small r, over blue, large r, curves). The transition between the two reflections

IET Radar Sonar Navig., pp. 1–9
doi: 10.1049/iet-rsn.2014.0206

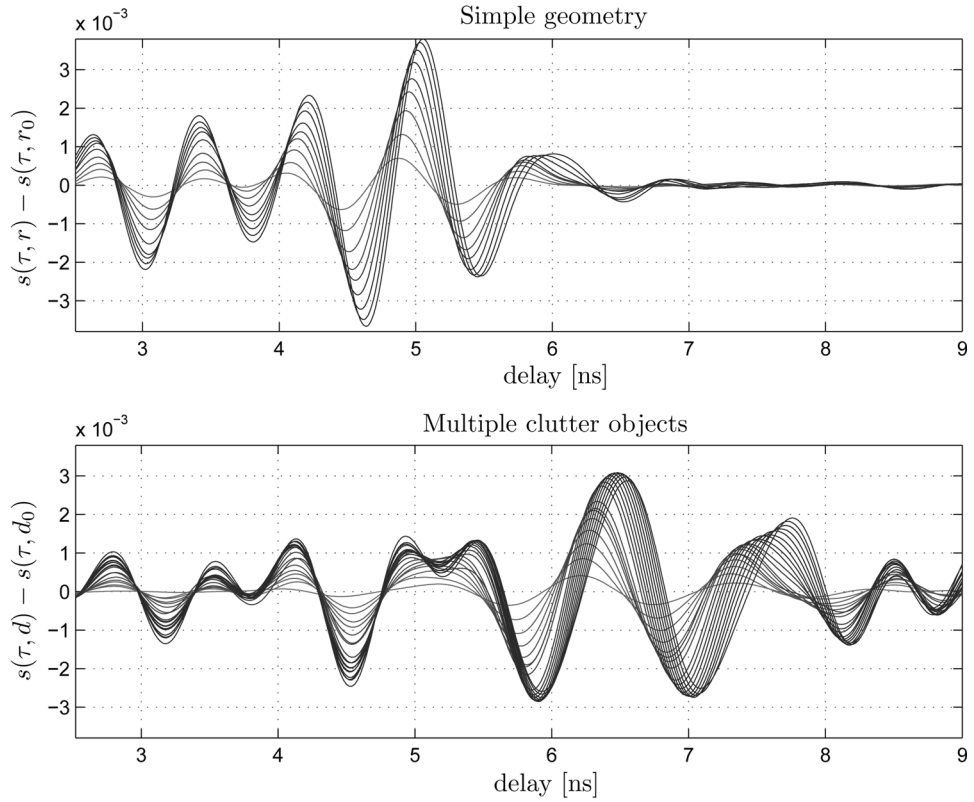

Fig. 4 *Dynamic echoes for the set of radii where the echo corresponding to that of smallest radius r_0 was used as reference*
The radius order was spanned from small (red) to large (blue)

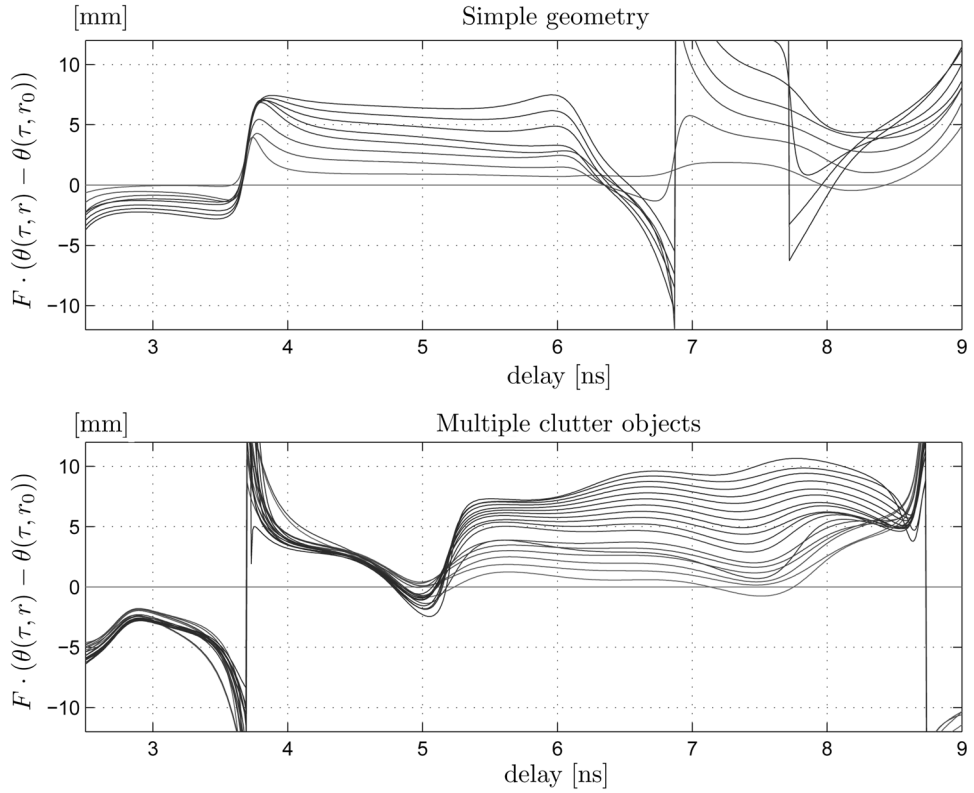

Fig. 5 *Scaled ($F = -c/(2\omega)$) phase difference of the analytic signal for the set of radii and as a function of delay (τ)*
The radius order was spanned from small (red) to large (blue). To unwrap the phase, it was initialised at 5.5 ns of delay and unwrapped independently towards small and large delays. The unwrapping was subject to errors of $n2\pi$

occurred at around 3.7 ns. Before this transition, the range decreased by approximately 2 mm for an approximately 4 mm change in radius (sensitivity $S \simeq -0.5$). After this transition, the range increased by approximately 7 mm for the same 4 mm change (sensitivity $S \simeq 1.75$). The sensitivity appeared to be linear: every equal change in radius leads to an approximately equal change in delay shift.

The zero-crossings within the reflections were approximately constant at 0.5 ns, suggesting a centre frequency of 1 GHz. The energy in the second reflection was greater.

4.1.2 Clutter objects: In the subsequent experiments, static objects were inserted into the model while keeping all else as close to the previous experiments as possible; although static, the clutter objects affected the radar signature because of indirect echoes via the dynamic tube.

The time domain was not easily classified into two regions based on sensitivity: the sensitivity evolves between positive and negative weak values before reaching large positive values at peak dynamic echo intensity. In this latter region, the sensitivity is in the range $S \in [0.9, 1.2]$.

The zero-crossings within the region of peak dynamic echo intensity are approximately constant at 0.6 ns, suggesting a centre frequency of 0.8 GHz.

With regards to signal strength, and based on considering the frequency domain data of the strongest dynamic echo, the round trip attenuation before subtraction of a reference echo was in the order of 50 dB at around 0.8 GHz. Previous simulation results have suggested 40 dB at around 1 GHz [16] at 10 cm depth and a 1 cm radius 'aorta'. These values were close when compensating for differences in liquid properties, 'aorta' diameter and depth.

4.2 Error sources experiments

With the complex environment and the apprehension of stray movements and possible clutter objects, a series of experiments were conducted aiming to exclude competing hypotheses: Was the dynamic radar echo dominated by the internal geometry – in particular the aorta – or did other factors preclude a clean observation?

The first observation was that the dynamic density had significantly larger values in the 'transversal' experiment compared with others.

Furthermore, the variations within this experiment were greater than for any other experiment, both with respect to amplitude and especially to delay shifts which were larger than for any other experiment.

The correlation between transversal position and delay was opposite in the interval between 1 and 2.5 ns compared to between 2.5 and 3.2 ns; this indicated at least two independent reflectors.

Although using the same geographical extent and similar influence, the 'longitudinal' experiment did not contain the amount of variation observed in the 'transversal' case, neither w.r.t. dynamic density amplitude nor w.r.t. delay shifts.

The echoes observed when re-mounting the equipment, re-attaching the antennas or even adding artificially an external reflector showed small variations, and these variations were essentially a question of dynamic density amplitude, less of delay shifts. Of particular importance was the external reflector experiment where variation was essentially equivalent to the 'attaching' experiment, suggesting that external reflectors did not significantly influence the dynamic echo (Fig. 6).

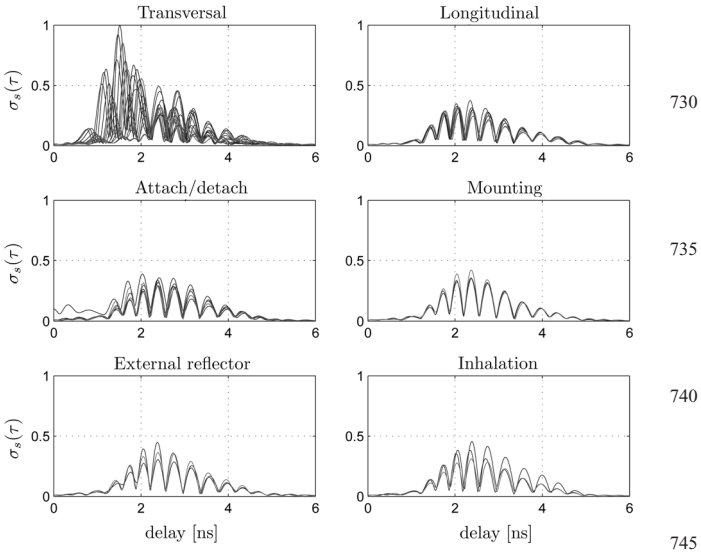

Fig. 6 *Set of dynamic densities $\left(\sigma_s^{(i)}(\tau)\right)$ for acquisition i, each associated with a hue between blue and red, grouped according to experiment 'Transversal', 'Longitudinal' and so on*

The variation in the dynamic density measures the influence of the factor varied over the set of acquisitions within an experiment

4.3 Human subject experiments

Owing to the large variation in the transversal experiment as compared with the other experiments, these data are investigated more in depth.

The results from the transversal experiment spanned 3.5 cm to each side of the origin of the coordinate system. The static and dynamic echoes exhibit a large degree of continuity as a function of transversal position (x, see Fig. 7). Continuous troughs and crests was interpreted as 'reflectors', although the shape and complexity of these 'reflectors' was not known.

In the static echoes, there are two dominant reflectors followed by indications of other reflectors, especially after around 2 ns. There was a component with negligible dynamic density between 0 and 1 ns: this component is the antenna coupling (direct path, 'DP').

In the stacked dynamic and static echoes, there was a first ('1st') reflector with curved delay with maximum close to the midpoint of the transversal positions. The strength of this component remains almost constant in the static echoes while it is greatly variable in the dynamic echoes, with a minimum at between −1 and −1.5 cm.

The strongly varying amplitude of the crest at around 2 ns in the static echoes suggests the presence of other reflectors at and around this delay with commensurate reflector strength. The dynamic echoes suggest at least two components denoted 'A' and 'B' in Fig. 7. The reflector 'B' has a curvature with closest delay at $x \simeq -1.5$ cm.

4.4 Radar imaging

The transverse experimental data are subject to an imaging process and the results are shown in Fig. 8. The images shown alongside an MR image correspond to the antenna locations. A time domain gating at around 2 ns separates the images into a 'near' image and 'far' image (larger delay). The 'near' image almost entirely contains the 'DP' and 'first' components whereas 'others' is mostly contained in the 'far' image.

A reflector was observed at approximately (−3 cm, 8 cm) ('left', see 'far' image in Fig. 8) and which corresponded

doi: 10.1049/iet-rsn.2014.0206

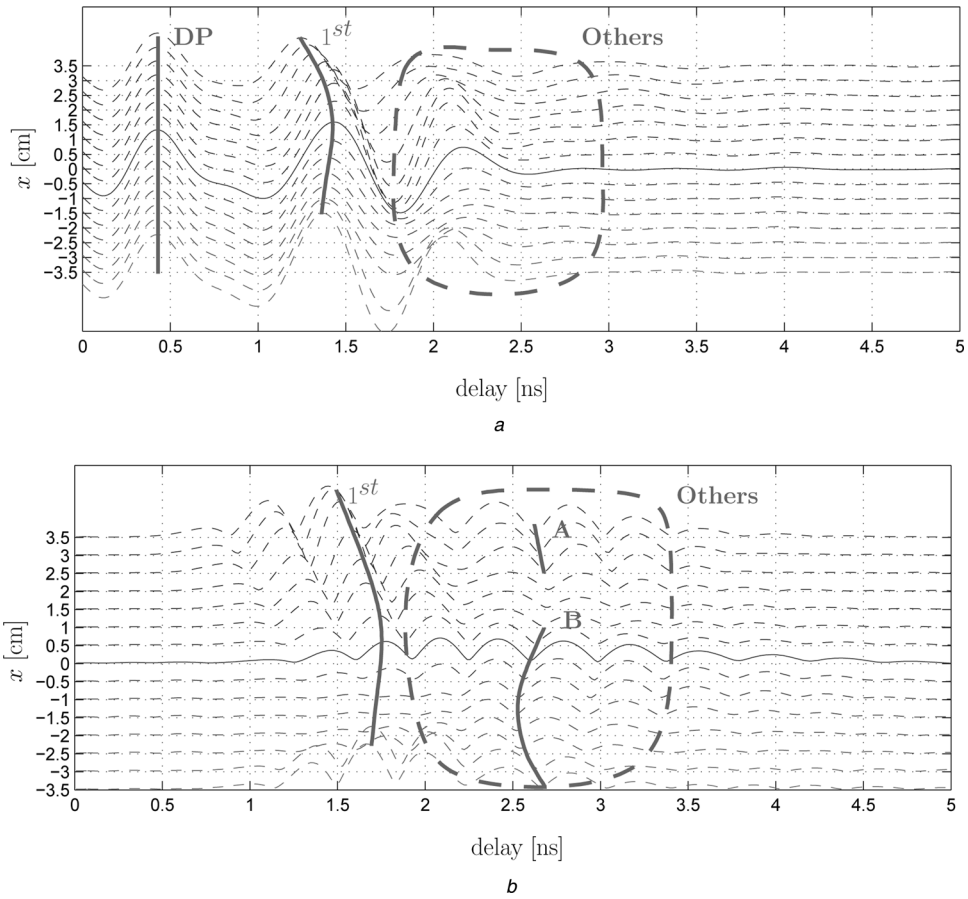

Fig. 7 *Stacked, static echoes ($E_t[s(\tau, t)]$ above) and dynamic density (σ_s below) as a function of transversal position x*

Reflectors are suggested in green based on continuity across channels or interference phenomena expressed as varying amplitudes of crests

a Static echoes

b Dynamic echoes

grossly to the location of the aorta in the MR image. The resolution of the imaging process is poor, due to both the low-pass filtering from tissue loss and the limited extent of the antenna positions. Despite this low resolution, the presence of reflectors at 'centre' (1 cm, 10 cm) and 'right' (6 cm, 8 cm) are likely.

The components in the 'near' image are much stronger than those in the 'far' image and show a grossly triangular shape which was collocated with the boundary between the ribs and lungs.

4.5 Slow time traces

To investigate the time-dependency of the dynamic echoes, the traces at different ranges and transversal locations, as well as traces in the imaging results have been studied.

The time-dependency of the dynamic echoes, at different ranges, generally do not suggest a systematic tendency of increasing shift in slow time as the trace corresponds to an increasing distance from the heart. A possible exception to this observation is shown in Fig. 9 where the shift did

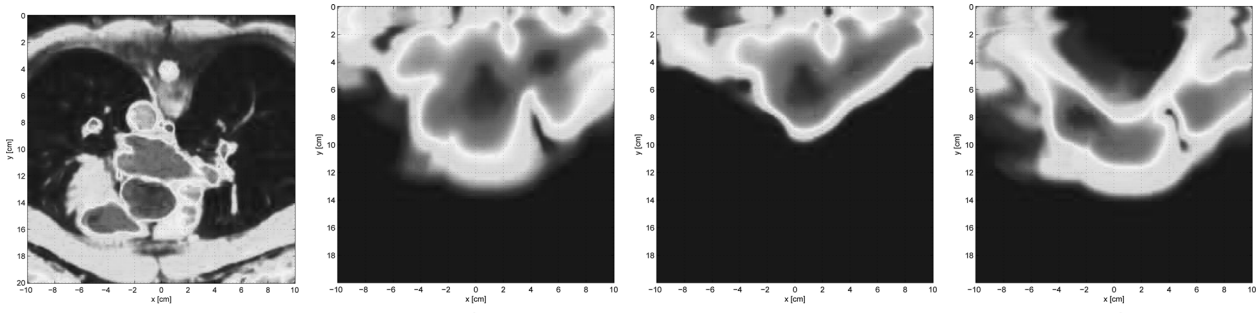

Fig. 8 *Dynamic radar images were compared to the relevant MR slice*

The dynamic image was in addition 'decomposed' based on time domain gating prior to image formation: [0.8, 2.0] ns for the 'near' image and [2.0, 5.0] ns for the 'far' image. The dynamic range was 50 dB

a xy slico of MR date

b Dynamic image

c Dynamic, 'near' reflectors

d Dynamic, 'far' reflectors

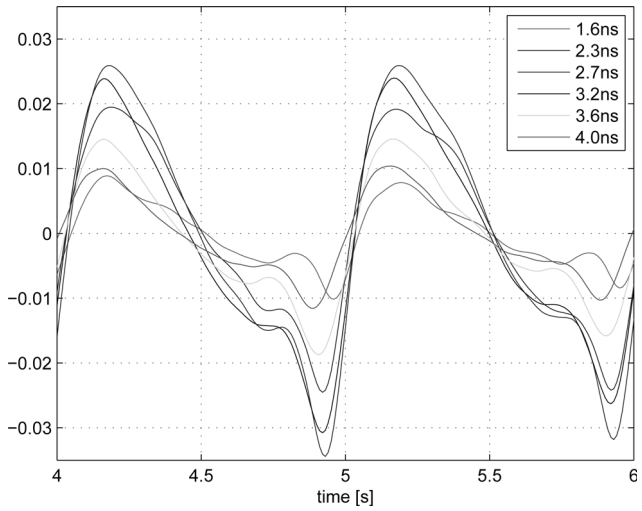

Fig. 9 *Traces extracted from the dynamic echoes at $x = -1.0$ cm*

The delay τ_i for each trace $s_\Delta(\tau_i, t)$ represents increasing range. Shifts between different traces is not likely due to acquisition noise: such noise affects each echo (t) in an acquisition independently

increase with diminishing range and where the maximum shift was not more than approximately 6% of the cycle, or approximately 57 ms.

5 Discussion

5.1 Phantom model

The experiments in a phantom model showed that two distinct 'reflections' could be identified with the tube when the clutter environment was weak. This separation was based on regions with distinct sensitivity with negative value for the first reflection and positive sensitivity associated with the second reflection. Also, the transition between reflections corresponded fairly well to the tube centre. This case was successful despite the model having greater loss at larger frequencies than was expected in human tissues. In this case, calculating a clear indicator of varying tube radius was considered feasible.

In a harsher clutter environment, the dynamic echoes could no longer be easily classified into two components: (i) Neither negative nor positive sensitivities were as strong; (ii) The negative sensitivities were practically zero; (iii) Where reflections were strongest, the sensitivity was greatest and positive. This was considered to be the expression of interference phenomena in a multipath environment.

A similar observation was reported in [19]: heterogeneous environments created propagation effects which lead to reduced sensitivity of the posterior reflection and thereby a stronger reduction given static echo suppression. Despite a widely different scattering environment between the phantom model and the simulations, the consequence was similar in that the first reflection was reduced and no reflectors with negative sensitivity were distinctly identified.

Despite these strong clutter environments, information was present regarding the radial variations and which could be used in an indirect scenario.

5.2 Human subject experiments

Although dynamic echoes were expected in the radar observations, its causes could have been diverse. We needed to identify echoes due to the aorta which were distinguishable from other sources.

Given the weak radar signals, a series of experiments were designed to rule out hypothetical 'error' sources, including external reflectors, and which showed that the dominant source of dynamic echoes was from variation in the transversal (x) direction. Combined with the continuity of these dynamic echoes across x, we concluded that the internal, geometric variation along x dominated dynamic echoes. The following considered this variation.

In both the stacked, dynamic echoes and in the radar images, strong indications of the aorta as a discernible reflector were to be found. First, in the radar images, a separate reflector was distinguished at a location close to where the aorta was expected based on MR images of the same region. Second, in the dynamic echoes, the reflector 'B' resembled the echo from a concentrated reflector: the curvature of its crest and troughs is of the correct form. Third, it was closest to the back at $x \simeq -1.5$ cm, which was where the aorta was expected to lie. And fourth, a delay of 2.5 ns corresponded to a depth around 7 cm, while the closest position of the aorta centroid was at around 7.5 cm according to the MR images.

For robust estimation of aortic radius, the aorta would be the dominant dynamic reflector within the relevant range; hence in [15], this hypothesis was investigated. This study showed: (i) movements of the arterial tree in the lungs at similar range and (ii) strong movements of the heart at larger range. Although not identified in [15], earlier dynamic reflectors were assumed to be due to the lungs–thoracic cage boundary. In the following, these influences on the aorta dynamic echo will be discussed.

Although the movements of the lung arteries were commensurate with that of the aorta in [15], as a reflector the aorta by its radius and straight, cylindrical shape was expected to dominate.

With respect to the heart echoes, very little dynamic power was perceived beyond 10–11 cm depth in the radar images; this was where the heart response was expected. It appears that despite the large size and strong movements of the heart, its echoes were not dominant in the radar acquisitions. The possible factors explaining this were the attenuation of electromagnetic signals, which increased with distance in addition to losses due to reflections at boundaries. Another factor was the small reflection coefficient between muscles and blood: it was primarily at such boundaries where the largest movements occurred.

With regards to the first ('1st') reflection, we believe that this was related to the boundary between the lungs and the ribs-muscles at the back: both the small range, the shape in the radar images and the 'extended reflector' interpretation (curvature of troughs and constant crest amplitude preclude a point-like reflector) in the static and dynamic echoes support such an interpretation. Since no discernible movement was detected at this interface in [15], a relatively large sensitivity of the radar echoes to this boundary's displacements was concluded: the small range implied a reduced attenuation in intermediate tissues as well as few reflective boundaries between antennas and lungs, and the size of the reflector was large. Although this component was the strongest dynamic reflector, the time-domain separation with the aorta echo appeared to be sufficient to extract information on the latter.

Although evidence of a distinct aorta echo seemed to be present in the dynamic echoes, no 'opposing' sensitivities were found and therefore no evidence of both posterior and anterior reflections was identified. As pointed out in the

doi: 10.1049/iet-rsn.2014.0206

phantom experiments, this is most probably due to interference phenomena. Another issue with the information relative to the aorta followed from an observation in [15]: the aorta radius was coupled with the aorta centroid. This meant that a single indicator of aorta variation contains information on both sources: centroid and radius. For blood pressure estimation, it would probably be necessary to separate the two sources; it is possible that acquiring echoes from the aorta at different z-levels can be used to such an end.

Hypothetically, the traces related to the aorta reflection could have contained information that allow for separating the influences if the radius variation occurred at a different time in the heart cycle than the propagation of the heart movement through the tissues at the back. However, the time separation of these traces as a function of the range of the traces showed no significant separation (Fig. 9). To obtain the same effect, in [15] the movement of the centroid appeared to large extent synchronous with the aorta radius variations. Furthermore, the average blood pressure pulse propagation speed in the arterial tree for a person around 40 years old is between 6 and 7 m/s [20]; assuming a distance of between 15 and 25 cm from the aortic valve to the relevant slice, this corresponded to a delay of 21–42 ms – grossly 2–4% of a cycle, and considered too small for separation.

A second factor that could have allowed for a separation is significant difference in shape of the traces. No such difference was perceived in the observed radar traces, nor was any expected given that the heart left ventricular created both the strongest mechanical coupling and the internal pressure wave in the aorta.

6 Conclusions

A discernible, dynamic reflector was identified and believed to be an echo from the aorta. This reflector was distinct from earlier, strong dynamic reflectors. Also, we concluded that direct heart reflections are weak.

However, in the aim of estimating aorta radius variations, two issues were identified, but distinct posterior and anterior reflections were not identified, which suggested that blood pressure estimation needed to rely on PWV, and the literature has shown that aorta size and centroid variations are coupled.

Future research could consider using simultaneous signatures from the aortic radius variations at several levels along the back in order to decouple aortic displacement and size.

7 Acknowledgment

This work was part of the MELODY project, which is funded by the Research Council of Norway under the contract number 187857/S10.

8 References

1 Parati, G., Ongaro, G., Bilo, G., *et al.*: 'Non-invasive beat-to-beat blood pressure monitoring: new developments', *Blood Pressure Monitor. (Workshop)*, 2003, **8**, pp. 31–36

2 Matthys, K., Verdonck, P.: 'Development and modelling of arterial applanation tonometry: a review', *Technol. Health Care*, 2002, **10**, pp. 65–76

3 Foo, J.Y.A., Lima, C.S.: 'Pulse transit time as an indirect marker for variations in cardiovascular related reactivity', *Technol. Health Care*, 2006, **14**, pp. 97–108

4 Sharwood-Smith, G., Bruce, J., Drummond, G.: 'Assessment of pulse transit time to indicate cardiovascular changes during obstetric spinal anaesthesia', *Br. J. Anaesthesia*, 2006, **96**, pp. 100–105

5 Droitcour, A.D.: 'Non-contact measurements of heart and respiration rates with a single-chip microwave Doppler radar'. PhD dissertation, Department of Electrical Engineering, Stanford University, June 2006

6 Sugawara, M., Niki, K., Furuhata, H., Ohnishi, S., Suzuki, S.-J.: 'Relationship between the pressure and diameter of the carotid artery in humans', *Heart Vessels (Short Communication)*, 2000, **15**, pp. 49–51

7 Lass, J., Meigas, K., Karai, D., Kattai, R., Kaik, J., Rossmann, M.: 'Continuous blood pressure monitoring during exercise using pulse wave transit time measurement'. Engineering in Medicine and Biology Society, 2004. IEMBS '04. 26th Annual Int. Conf. IEEE, September 2004, vol. 1, pp. 2239–2242

8 Stuchly, S., Goldberg, M., Thansandote, A., Carraro, B.: 'Monitoring of arterial wall movement by microwave Doppler radar'. Symp. on Electromagnetic Fields in Biological Systems, Ottawa, Canada, 27–30th June 1978, pp. 229–242

9 Papp, M., Hughes, C., Lin, J., Pouget, J.: 'Doppler microwave – a clinical assessment of its efficacy as an arterial pulse sensing technique', *Investig. Radiol.*, 1987, **22**, pp. 569–573

10 Massagram, W., Lubecke, V.M., Host-Madsen, A., Boric-Lubecke, O.: 'Assessment of heart rate variability and respiratory sinus arrhythmia via Doppler radar', *IEEE Trans. Microw. Theory Tech.*, 2009, **57**, (10), pp. 2542–2549

11 Aardal, Ø., Hamran, S.-E., Berger, T., Paichard, Y., Lande, T.S.: 'Chest movement estimation from radar modulation caused by heartbeats'. IEEE Biomedical Circuits and Systems Conf., November 2011, pp. 422–425

12 Lu, L., Li, C., Lie, D.Y.C.: 'Experimental demonstration of noncontact pulse wave velocity monitoring using multiple Doppler radar sensors'. Annual Int. Conf. IEEE EMBS, August 2010, pp. 5010–5013

13 Lin, H.-D., Lee, Y.-S., Chuang, B.-N.: 'Using dual-antenna nanosecond pulse near-field sensing technology for non-contact and continuous blood pressure measurement'. 34th Annual Int. Conf. IEEE EMBS, August 2012, pp. 219–222

14 Stefanidis, C., Stratos, C., Vlachopoulos, C., *et al.*: 'Pressure-diameter relation of the human aorta. A new method of determination by the application of a special ultrasonic dimension catheter', *Circulation*, 1995, **92**, pp. 2210–2219

15 Solberg, L.E., Balasingham, I., Fosse, E., Hol, P.K.: 'Heart-induced movements in the thorax as detected by MRI'. Available at: http://arxiv.org/abs/1405.6747, 2014

16 Solberg, L.E., Balasingham, I., Hamran, S.-E., Fosse, E.: 'A feasibility study on aortic pressure estimation using UWB radar'. IEEE Int. Conf. Ultra-Wideband 2009, September 2009, pp. 464–468

17 Berger, T., Hamran, S.-E., Paichard, Y., Aardal, Ø.: 'Close range ultra wideband microwave imaging in a non-homogeneous background'. Proc. IASTED Int. Conf. Signal and Image Processing, December 2011, pp. 188–194

18 Gabriel, S., Lau, R.W., Gabriel, C.: 'The dielectric properties of biological tissues: III. Parametric models for the dielectric spectrum of tissues', *Phys. Med. Biol.*, 1996, **41**, pp. 2271–2293

19 Solberg, L.E., Balasingham, I., Hamran, S.-E.: 'Realistic simulations of aorta radius estimation'. Proc. Fourth Int. Symp. on Applied Sciences in Biomedical and Communication Technologies, Barcelona, October 2011, article no. 47

20 The Reference Values for Arterial Stiffness' Collaboration: 'Determinants of pulse wave velocity in healthy people and in the presence of cardiovascular risk factors: 'establishing normal and reference values'', *Eur. Heart J.*, 2010, **31**, (19), pp. 2338–2350

www.ietdl.org

RSNSI20140206

Author Queries

Lars Erik Solberg, Øyvind Aardal, Tor Berger, Ilangko Balasingham, Erik Fosse, Svein-Erik Hamran

Q1 Please check the email id of the corresponding author.

Q2 Please note that the references are renumbered to be in numerical order as per the journal style.

Q3 Figure 2 is uncited. Please check the inserted citation and placement.

Q4 Is 5 through 7 referring to steps V to VII. If so, can we change it to V–VII.

Q5 As per journal style colour figures are not allowed. We have changed to greyscale format. Please check amend it in text accordingly.

Q6 Figure 6 is uncited. Please check the inserted citation and placement.

Q7 Please check insertion of subcaption Figs. 7 and 8.